Geophys. J. Int. (1995) **123,** 169–182

The contrast in upper mantle shear-wave velocity between the East European Platform and tectonic Europe obtained with genetic algorithm inversion of Rayleigh-wave group dispersion

Anthony Lomax and Roel Snieder
Department of Theoretical Geophysics, Utrecht University, PO Box 80.021, 3508 TA *Utrecht, The Netherlands*

Accepted 1995 April 26, Received 1994 November 9; in original form 1994 August 25

SUMMARY

The stable, Precambrian East European Platform adjoins the younger, tectonically active regions of central and western Europe along a distinct crustal boundary, the Tornquist–Teisseyre Zone (TTZ). Seismic body- and surface-wave studies indicate that there may be a significant change in *S*-wave velocity at the top of the mantle in the region of the TTZ, with higher velocities under the East European Platform. To confirm these results we use a genetic algorithm (GA) to invert fundamental Rayleigh group-velocity estimates for wave paths across western and central Europe and across the East European Platform to determine 'average' layered *S*-velocity models separately for each region. The use of the GA method allows identical model parametrizations and broad parameter search ranges to be used for both regions so that a relatively unbiased estimate of the difference in structure can be obtained.

The GA is a guided search technique which requires neither a linearized forward method nor a single starting model and which can be applied to very large model-spaces. Consequently, fewer assumptions and physical approximations are required and a greater range of possible solutions is examined than with many other inversion methods. Here we employ the GA to produce a large set of acceptable solutions and associated misfit values, in contrast to inversion for a single, 'optimum' solution. The scatter in the set of acceptable solutions gives an estimation of uncertainty, resolution and parameter trade-offs of the non-linear inversion.

The scatter of the solutions for the dispersion data shows velocity–depth trade-offs around the Mohorovičić discontinuity, indicates the maximum depth resolution of the inversion, and shows the uncertainty in upper mantle *S*-velocity estimates. The results indicate a thicker crust and up to $0.3\,\mathrm{km\,s^{-1}}$ (7 per cent) higher 'average' *S*-wave velocities in the upper 100 km of the mantle under the East European Platform than under western and central Europe.

Key words: Europe, genetic algorithms, inversion, mantle structure, surface waves.

INTRODUCTION

In western Eurasia there is a striking juxtaposition of stable, Precambrian continental crust, the East European Platform, against the younger, tectonically active continental and oceanic regions of central and western Europe and the western Mediterranean, referred to here as tectonic Europe. The East European Platform (EEP) adjoins tectonic Europe (TE) along or near the NW–SE-trending Tornquist–Teisseyre zone (TTZ, Fig. 1) and nearby structures such as the Sorgenfrei–Tornquist Zone, the Trans-European Fault and the eastern margin of the Carpathian Mountains (Blundell, Freeman & Mueller 1992). The TTZ is a zone of tectonic disruption whose surface expression falls along a relatively narrow zone of about 100 km or less; geophysical studies indicate that it involves the whole thickness of the crust, separating 25–35 km thick crust under TE from 40–55 km thick crust under the EEP (Guterch *et al.* 1986; Meissner 1986; Blundell *et al.* 1992). However, the existence of and character of a change in upper mantle structure across the TTZ are more difficult to determine.

The results of Zhang & Tanimoto (1993) for high-resolution global inversion for lateral variation in *S* velocity show a region of anomalously high velocity under the Baltic Shield and EEP in depth sections at both 110 and 210 km. This high-velocity region is bounded to the south-west by a relatively sharp transition along a line roughly coincident with the TTZ;

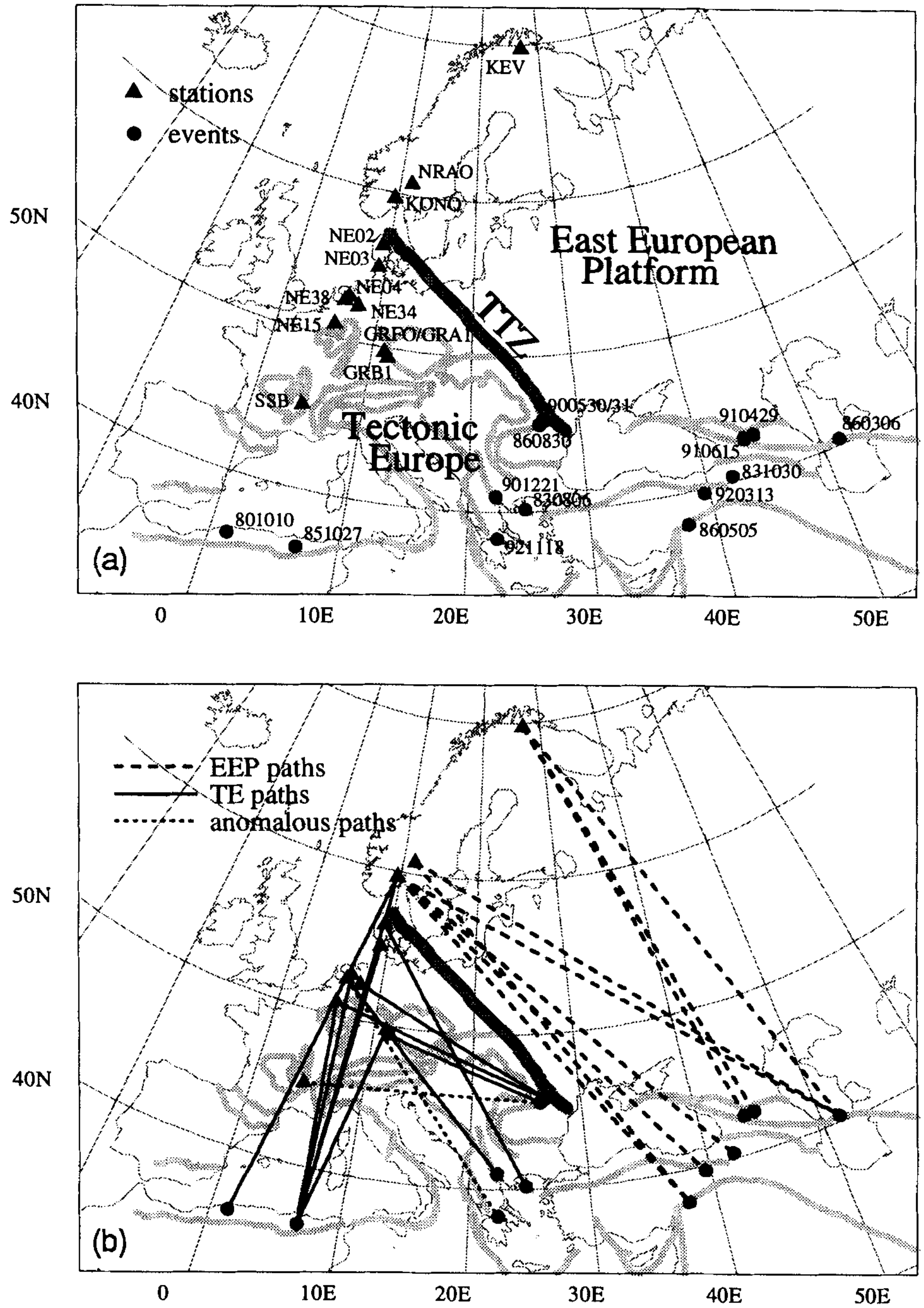

Figure 1. (a) Map showing major tectonic boundaries (medium-width grey lines), Tornquist–Teisseyre Zone (TTZ, thick grey line), stations (▲) and events (●). (b) Great circle paths between sources and receivers for observed seismograms used in this study. Long dashed lines indicate paths used for EEP inversion; solid lines indicate paths used for TE inversion. The short dashed lines in TE indicate the paths that produce anomalous dispersion estimates.

the maximum contrast across this boundary is about 4 per cent. Regional *S* body- and surface-wave studies indicate a contrast of up to 10 per cent in *S*-wave velocity at the top of the mantle in the region of the TTZ, with higher velocities under the EEP (Snieder 1988; Zielhuis & Nolet 1994). *P* body-wave studies also indicate increased *P*-wave velocity under the EEP (Hurtig, Grässl & Oesburg 1979; Spakman, van der Lee & van der Hilst 1993).

In particular, the 'partitioned waveform' *S*-velocity inversion of Zielhuis & Nolet (1994) at 80 km depth and a *P*-velocity tomographic inversion of Spakman *et al.* (1993) at 145 km depth both show a change in velocity along a zone nearly coincident with the surface expression of the TTZ. However, in both of these studies, the spatial coverage of the observations is poor to the north-east of the TTZ, so it is not clear if the velocity change near the TTZ continues to the north-east and how this velocity change is related to the larger-scale velocity structure for the EEP.

In this paper, we begin with the hypothesis that there may be some regional change in 'average' uppermost mantle *S* velocity across the TTZ, as indicated by the earlier studies. We use a genetic algorithm (Lomax & Snieder 1994) to determine two sets of layered, S-velocity models which produce fundamental-mode Rayleigh group-velocity dispersion curves which most closely match the group-velocity data for wave paths on each side of the TTZ. The observations are digital seismograms from NARS and GDSN stations in northern Europe from events located primarily to the south-east of Europe and recorded at distances of about 10°–30° (Fig. 1). Our purpose is to confirm the earlier results with extension of the study region further to the north-east, and to exploit the potential of genetic algorithms to constrain the extent to which the average velocity models differ.

GENETIC ALGORITHM INVERSION OF GROUP-VELOCITY DISPERSION

We choose a genetic algorithm (GA) to invert the group-dispersion data because it allows a fully non-linear search of a large solution space and because it produces a set of acceptable solutions (Keilis-Borok & Yanovskaya 1967; Lomax & Snieder 1994) which give a useful and direct presentation of the uncertainty and trade-offs in the results. The GA method (Goldberg 1989; Holland 1992) is one of a number of newer search techniques that can give an efficient sampling of a large model space; recently it has been used often in geophysics (e.g. Stoffa & Sen 1991; Sen & Stoffa 1992; Sambridge & Drijkoningen 1992; Jin & Madariaga 1993; King 1993; Nolte & Frazer 1994). The GA method is a guided search which operates with populations of trial solutions to construct succeeding populations, or generations, in which on average there will be solutions with lower 'misfit'. This misfit is found by applying the forward method to a trial solution to produce predicted data and then performing some comparison with the real data.

In the GA employed here, a trial solution consists of a set of m parameters. Each parameter is specified by n bits, giving 2^n possible values for the parameter. Different parameters may be specified by a different number of bits. Within the GA, a solution is represented by a *bit string* constructed from some binary representation of all m parameters. If there are N total bits in a bit string, then there will be 2^N possible solutions for the discretized problem. The GA itself operates only with the binary bit strings and associated misfit values; the physical meanings and values of the parameters are used outside the GA in a separate routine which applies the forward method and calculates the misfit.

Beginning with a random initial population of solutions and corresponding misfits, succeeding populations are created by

(1) *selection*: saving those solutions with smaller misfit;
(2) *crossover*: combining parts of two solutions to form new trial solutions; and
(3) *mutation*: changing the values of the parameters of a solution.

All three of these operations are controlled stochastically. New populations are created for a fixed number of generations or until some misfit reduction criterion is reached. The GA search produces a large set of solutions which give an estimate of the misfit surface in the model space.

Many interesting inverse problems in geophysics are non-linear and poorly constrained. Such problems may have multiple, broad or topologically complex regions of minimum misfit in the solution space. Our experience and other work (e.g. Goldberg & Richardson 1987; Stoffa & Sen 1991; Nolte & Frazer 1994) indicate that with this type of problem, each run of a GA tends to converge to a single, local minimum, and in different runs different minima may be found depending on the parameters controlling the GA search operations. Such convergence to a local minimum not only prevents the identification of all acceptable solutions, but also may produce a highly localized, poorly distributed set of solutions that is not appropriate for later statistical analyses or for use as an estimate of the *a posteriori* probability density function for the inversion (see Sen & Stoffa 1992; Nolte & Frazer 1994).

Many GA applications converge to a single, local minimum because they are configured for rapid convergence with the goal of finding an 'optimum' solution. Here, the GA is configured to attempt to find sets of acceptable solutions; solutions representing all regions of the model space that give a misfit with the data below some level (Fig. 2; Keilis-Borok & Yanovskaya 1967; Lomax & Snieder 1994). We begin with a GA similar to that described by Sambridge & Drijkoningen (1992), but make the following changes.

(1) The rates of crossover and mutation are set relatively low so that many solutions pass unchanged to the next generations (crossover rate = 0.2, mutation rate = 0.2).

(2) The mutation rate controls the proportion of *strings* that are mutated, and, when a string is mutated, a single bit in every parameter is changed (so the effective mutation rate comparable to the values given in, for example, Sambridge & Drijkoningen (1992) is 0.025).

(3) The best solution of each generation is never explicitly carried over to the next generation (no *elitism*; see Goldberg 1989).

In addition, we define a minimum misfit 'cut-off' value and reset lower misfits to this value; this helps to prevent the stalling of the GA in deep minima that are much lower than the acceptable level (Fig. 2). This cut-off makes the GA more of a *stochastic* search and less of an *optimization* method for regions of the solution space with misfit below the minimum value. Based on preliminary comparisons, these adjustments tend to produce a smaller but more diverse and reproducible set of acceptable models relative to a GA configured for rapid

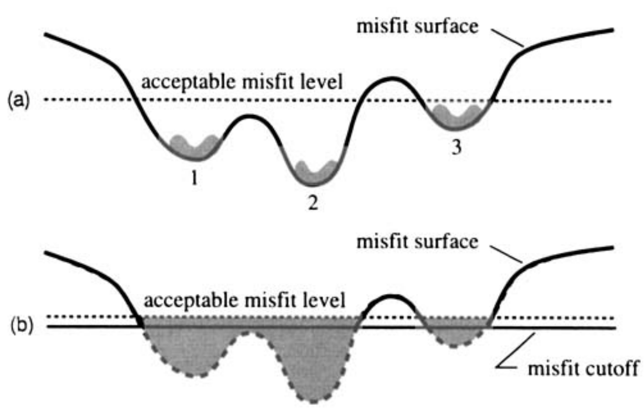

Figure 2. (a) A standard GA may find solutions located near only one of the minima 1, 2 or 3 in the misfit surface. But a goal of geophysical inversion is to find all solutions with a misfit below some acceptance level (e.g. data variance); all such solutions may give useful information about the problem. (b) A GA with a misfit cut-off at or below the acceptable level can aid in identifying a representative sample of acceptable solutions and avoiding deep local minima.

convergence. Similar effects on the behaviour of the GA might be obtained with other adjustments to the algorithm such as sharing (Goldberg & Richardson 1987; Goldberg 1989); and further work on the construction of GAs in the geophysical context is justified.

OBSERVATIONS

The observations for this study are digital seismograms from large earthquakes located primarily to the south-east of Europe and recorded at distances of about 10°–30° at NARS and GDSN stations in northern Europe (Fig. 1; Table 1). The seismograms were selected based on the location of the path between the source and receiver and on the signal-to-noise ratio of the surface waves. In general, large ($M_s > 5.5$), shallow events with a useful signal at above 100 s period are required to obtain resolution of the upper mantle with fundamental-mode surface waves. Unfortunately, because of the relatively short epicentral distances and the limitations of older digital recordings, many potentially useful seismograms were rejected due to clipping and other problems.

The event-stations paths obtained for the EEP give coverage of this region from just east of the TTZ to a distance of about 1500 km east of the boundary (Fig. 1). The ends of these paths extend into the Baltic Shield to the north, and into the Arabian–Eurasian collision zone to the south, but the greater part of all these paths lies within the EEP. The path coverage for TE is not so ideal. These paths cross diverse tectonic regions including the western Mediterranean, the Alps, the Rhine Graben and the Pannonian Basin. Also the average path length in TE is less than for the EEP, which leads to poorer group-velocity estimates at longer periods.

GROUP-VELOCITY ESTIMATION

Group dispersion for the fundamental Rayleigh mode is estimated from the observed waveforms using multiple-filter analysis (MFA) (Dziewonski, Bloch & Landisman 1969). The MFA procedure is applied to the observed seismograms after the instrument response has been removed, creating a set of envelopes of narrow-band seismograms. The data used for the GA inversion consist of group-velocity values at the peaks of the envelopes of the narrow-band seismograms at each period (Fig. 3). Only strong peak values which show reasonable group velocities for the fundamental Rayleigh mode are selected. We do not fit smooth dispersion curves through these data points because, first, the inversion includes a curve fit to the data, and, secondly, because the scattered data values give a frequency-dependent weighting to the inversion.

Following the procedure outlined above, fundamental Rayleigh group-velocity dispersion estimates within the period range of 7–300 s are obtained from vertical- and radial-component seismograms for the paths in both regions (Fig. 4).

When divided by region, the group-velocity dispersion estimates form two groups which, despite their overlap and scatter, have distinctly different characters (Figs 3 and 4). Relative to the EEP data, the TE data show generally higher group velocities in the range of 18–40 s, and lower velocities at periods greater than 50 s. Between about 50 s and 120 s the EEP data show an increase in group velocity with increasing period, while the TE data show constant or decreasing velocity in the same period range. The grouping of the data indicates that their inversion may resolve significant differences in 'average' crustal and upper mantle structure between the East European Platform and tectonic Europe.

An exception to this grouping is found for N–S paths from an event in Greece (event 1992 November 18) to NARS stations in and around the Netherlands and for an E–W path from Rumania (event 1986 August 30) to station SSB in southern France (short dashed lines in Fig. 1). For these paths, the group velocities for the fundamental-mode Rayleigh at periods representing the crust–mantle transition region (about 20–50 s) are about 0.25 km s^{-1} lower than those found for the other TE paths and more closely match the EEP dispersion data. The anomalous group dispersion found for these paths may be due to a number of factors, including variations in crustal thickness or multipath interference due to lateral variations in structure. In the 3-D inversions of Zielhuis & Nolet

Table 1. Event parameters.

year mo day	origin time	lat	lon	depth	m_b	M_s	region*	stations
1980 10 10	12:25:23.5	36.20	1.35	10	6.5	7.3	CE	kono
1981 10 28	04:34:17.8	-31.27	-110.65	10	6.2	6.2	PAC	jas
1983 08 06	15:43:51.2	40.14	24.77	2.4	6.2	7.0	CE	ne02
1983 10 30	04:12:27.1	40.33	42.19	12	6.1	6.9	EEP	kono
1985 10 27	19:34:57.1	36.40	6.75	10	5.5	5.9	CE	gra1,kono,ne03,ne04,ne15
1985 12 25	15:42:42.4	62.08	-124.15	10	5.7	5.0	CAN	rscp
1986 03 06	00:05:38.4	40.39	51.53	33	6.2	6.2	EEP	kev,kono,nrao
1986 05 05	03:35:38.8	37.97	37.77	10	5.8	5.9	EEP	kono,nrao
1986 08 30	21:28:36.0	45.55	26.30	139	6.3	6.9	CE	grb1,ssb†
1989 10 18	00:04:15.2	37.04	-121.88	19	6.5	7.1	PAC	kip
1989 12 25	14:24:32.6	60.08	-73.45	5	6.2	6.3	CAN	hrv
1990 05 30	10:40:06.2	45.87	26.67	90	6.7	--	CE	ne34
1990 05 31	00:17:48.4	45.80	26.75	96	6.1	--	CE	ne15
1990 06 10	05:00:54.6	62.36	-124.25	10	5.1	4.6	CAN	hrv
1990 12 21	06:57:44.0	40.98	22.34	18	5.8	5.9	CE	ne38
1991 04 29	09:12:47.3	42.49	43.65	9.6	6.2	7.0	EEP	kev
1991 06 15	00:59:20.4	42.44	43.99	10	6.0	6.1	EEP	kev
1992 03 13	17:18:40.2	39.71	39.57	28	6.2	6.8	EEP	kono
1992 06 28	11:57:34.1	34.20	-116.50	1	6.2	7.6	PAC	kip
1992 11 18	21:10:40.9	38.30	22.43	10	5.9	5.7	CE	ne38†

*CE, Central Europe; EEP, East European Platform; PAC, Pacific Ocean; CAN, Canadian Shield.
†Not used in inversion.

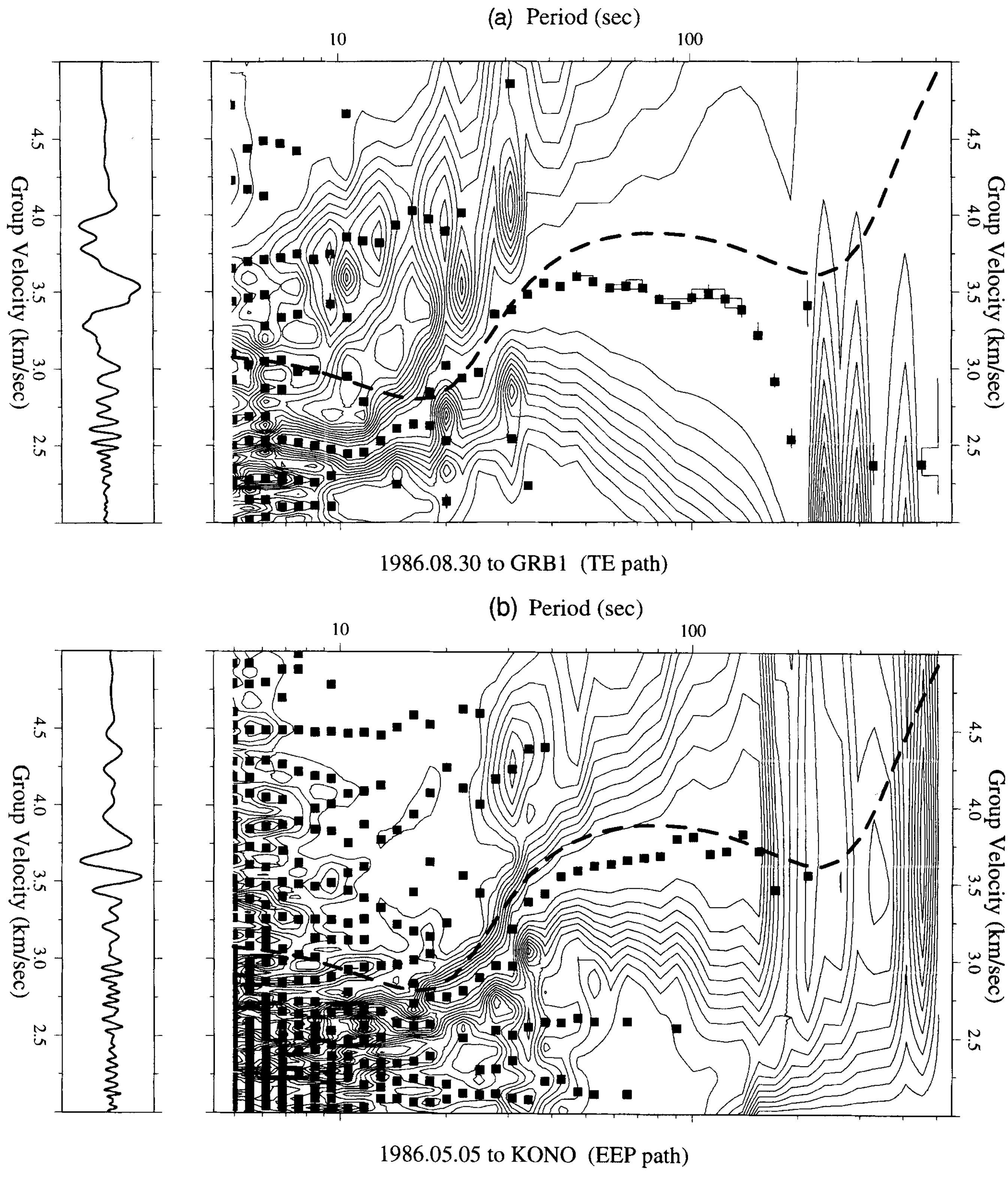

Figure 3. Group velocity versus period spectrograms from MFA analysis for vertical-component, long–period seismograms for two paths close to and on opposite sides of the TTZ. Records from (a) station GRB1 for event 1986 August 30 (TE path) and (b) station KONO for event 1986 May 5 (EEP path) are shown; these results are representative of the quality of the data set as a whole. Contours show the amplitude of the normalized envelopes of narrow-band, Gaussian-filtered seismograms at each period. Solid squares show the peaks of the envelopes at selected periods; the maximum peak values between 7 and 135 s for the GRB1 data and between 18 and 150 s for the KONO data were used for inversion. The heavy dashed line shows the fundamental-mode Rayleigh dispersion curve for the iasp91 model. The unfiltered, displacement seismograms plotted as a function of group velocity are shown to the left of each spectrogram.

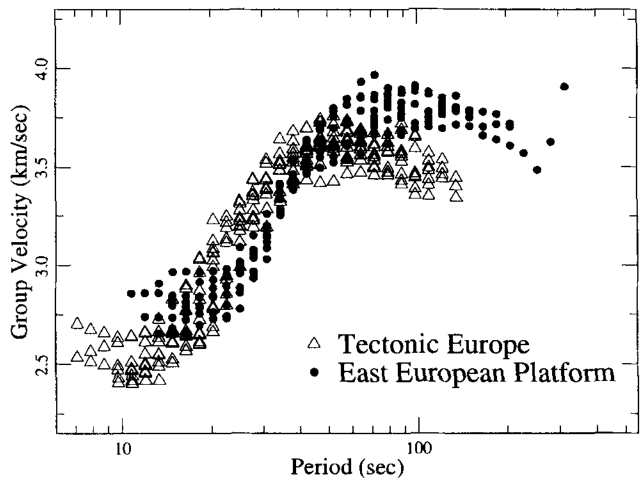

Figure 4. Fundamental-mode Rayleigh group-velocity estimates as a function of period from MFA analysis for wavepaths in TE and in the EEP.

(1994) and Spakman *et al.* (1993), relatively strong lateral variations in velocity are found for the region north of Greece, and Zielhuis & Nolet (1994) obtain relatively poor fits to the Rayleigh wave data from paths passing through this region. Both anomalous paths pass near the Alps where the crustal and Moho structures may be highly complex, including the deepest Moho depths under TE (up to 60 km) and possibly step offsets in Moho depth of about 10 km, stacking of crustal sections and detachment of lower crust into the mantle (Meissner 1986; Blundell *et al.* 1992). Since the other TE paths, which include continental regions adjacent to the TTZ, and to the east, north and west of the Alps, as well as a portion of the western Mediterranean, all have higher group velocities at crust–mantle transition periods, they are taken here as representative for TE. The anomalous Greece–Netherlands and Rumania–France data are excluded from this inversion; they should be re-examined later in a work that includes smaller-scale lateral velocity variations. The dispersion estimates for these paths at longer periods representing the mantle response are similar to those from other TE paths; consequently, the determination of an 'average' upper mantle structure for TE would not be affected strongly by the anomalous dispersion data.

MODEL PARAMETRIZATION

The GA technique, because it operates only with the binary solutions strings and their misfit values, places no restrictions on the physical aspects of the model parametrization. Any model parametrization that is compatible with the forward method can be used in the inversion. Since the GA technique can efficiently search a very large model space, the model characteristics can be liberally defined, with few assumptions and restrictions. This procedure will in general lead to a large number of solutions, but additional processing, constraints or assumptions can be used after inversion to limit the solution set further, if necessary.

In this study the same model parametrization and parameter search range are used for the inversion of the data from each side of the TTZ to allow a relatively unbiased comparison of the results from each region. This model is defined by four 'crustal' and 14 'mantle' S-velocity–depth nodes and a variable crustal thickness of between 15 and 70 km (Fig. 5). The crustal nodes are located at the surface, at 1 km depth, half-way between 1 km and the base of the crust, and at the base of the crust. The mantle nodes are spaced from the base of the crust to the bottom of the model at 2371 km depth. The spacing between mantle nodes increases approximately in proportion to the depth of the nodes; the distance between the top two mantle nodes is set to 0.35 times the crustal thickness. The location of the deepest crustal node and the shallowest mantle node at the same depth allows a step discontinuity (Moho) between the crust and mantle. The S velocity at each node can vary within the limits of approximately $\pm 1\,\mathrm{km\,s^{-1}}$ (about ± 20 per cent) of the S velocity from the iasp91 model (Kennett & Engdahl 1991) at the corresponding depth. The P velocity is determined from the S velocity using a Poisson's ratio of 0.25; the density profile is fixed for the crust and mantle and corresponds approximately to the values given in iasp91. The Moho-depth and S-velocity parameters are discretized with a very small step size, giving an effectively continuous variation between the limiting values. This parametrization gives about 10^{45} possible models, though the number of significantly different models is of the order of 10^{10} to 10^{20}. (For comparison, in a similar study using phase-velocity dispersion, Calcagnile & Panza (1978) employ a grid-search technique in a model space of about 2×10^4 crust/mantle models.)

A centrally weighted, five-point smoothing-over velocity is

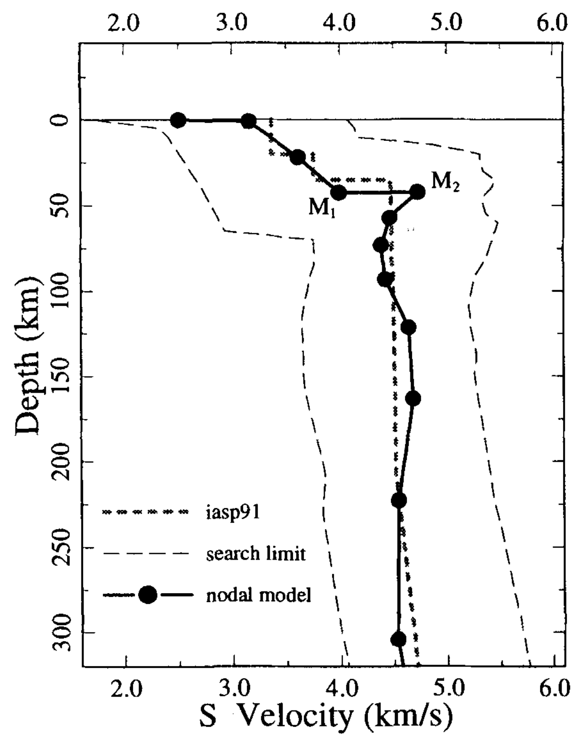

Figure 5. Velocity–depth diagram to 325 km depth showing the iasp91 S-velocity model, approximate search limits, and a sample of the nodal-model parametrization after five-point smoothing; the complete nodal model extends to 2371 km depth. The two nodes M_1 and M_2 at the same depth form a 'Moho' discontinuity which divides the nodal model into 'crust' and 'mantle' sections; the depth of these two nodes is a parameter of the inversion. The search limits show the extremal velocity values of the nodes from 1000 randomly generated models; the absolute search limits are broader than these approximate limits.

applied separately to the crust and mantle sections of the node model to suppress node-to-node oscillation of the solution. In addition, this smoothing suppresses steep velocity gradients at the top of the mantle, so that the step discontinuity allowed between the crustal and mantle nodes will form the principal boundary between the crust and mantle. The selection of this smoothing, like other forms of regularization, is somewhat subjective, and presents the risk of excluding some physically reasonable and scientifically illuminating solutions. The smoothed nodal model is used to calculate synthetic dispersion curves by solving the eigenvalue problem for Rayleigh waves as described by Takeuchi & Saito (1972) with corrections for a spherical earth. A random starting population of models for the GA search is shown in Fig. 6.

DEFINITION OF ACCEPTABLE MODELS

In this work, acceptable models are defined as those models giving predicted group-velocity values with an rms misfit in group velocity less than $0.85E_d$, where E_d is the rms of the differences in group velocity between each of the data values and all the other data values at each period. This definition of acceptance level is chosen so that the scatter of acceptable dispersion curves falls within the average scatter of the data. The minimum misfit cut-off level for the GA inversion is set to $0.75E_d$ so that an adequate number of acceptable solutions is obtained.

TEST WITH NOISY SYNTHETIC DATA

To check the accuracy of the group-velocity estimation and the GA inversion for a laterally homogeneous model, we apply the complete inversion process to a synthetic seismogram. First, we generate vertical-component, long-period seismograms for the fundamental Rayleigh mode from a shallow, double-couple source recorded at a distance of 30° in the layered earth model iasp91 (Kennett & Engdahl 1991). Next, we find the group-velocity dispersion estimates for the fundamental mode using the MFA procedure as described above. Then, we add realistic noise to these group-velocity estimates by taking the scattered EEP group-velocity estimates at each period and shifting them so that their mean value matches the MFA estimate for the isap91 synthetic seismogram. This results in a new, noisy group-velocity data set with the same number of data points and scatter at each period as the EEP data, but with a mean velocity at each period corresponding to the MFA estimates for the synthetic seismogram from the iasp91 model. We then invert the noisy data set using the model parametrization and GA procedure described above, with the expectation that the iasp91 S-velocity distribution will be contained within the scatter of acceptable models. Note that this test does not use exact parametrization—the input iasp91 model cannot be represented exactly by the nodal models used for inversion.

The results of the GA inversion of the synthetic seismograms are shown in Fig. 7. The distribution of acceptable models and corresponding dispersion curves shows the mapping of uncertainty between the data space and the model space. (Recall that acceptable models are defined as those models giving predicted group-velocity values with an rms misfit in group velocity less than $0.85E_d$.)

The large scatter of acceptable solutions at the top of the crust, the top of the mantle, and below about 350 km in the mantle indicate regions of model space that are not well

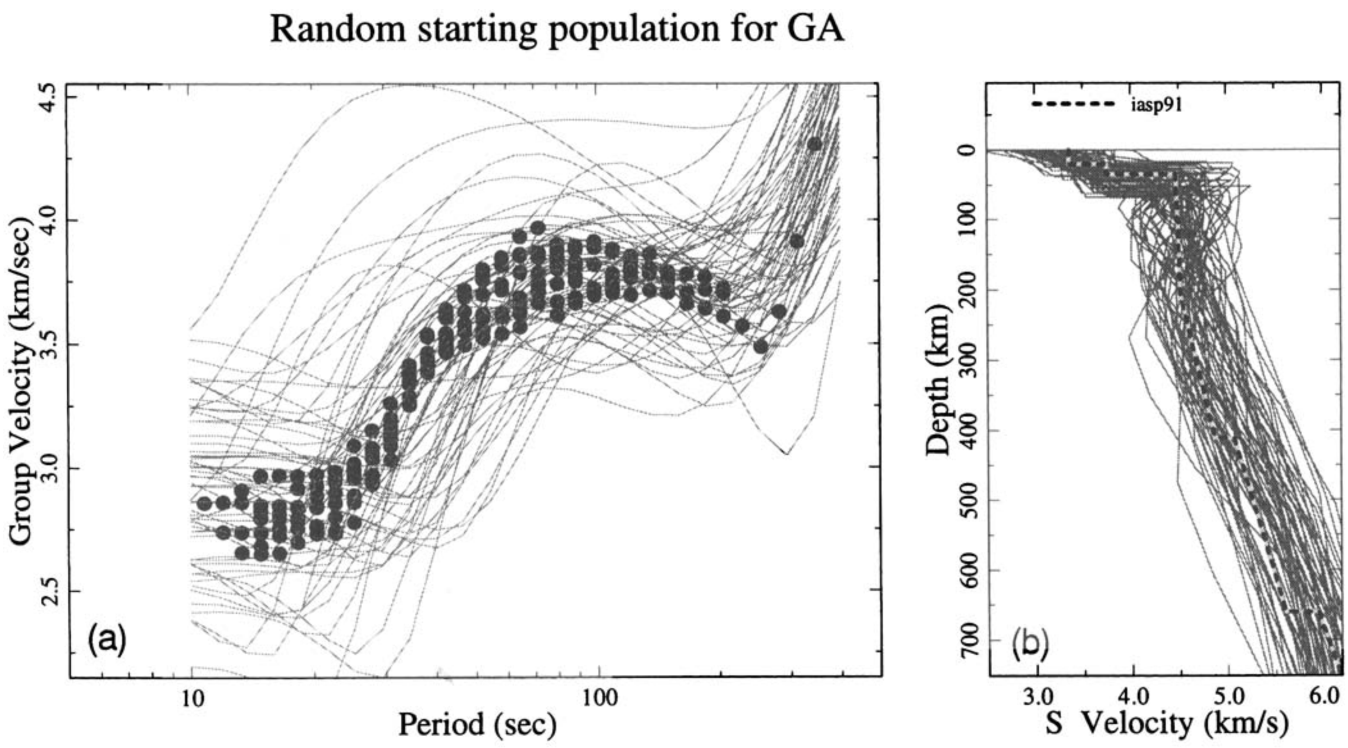

Figure 6. A random starting population of layered earth models (a) and corresponding synthetic dispersion curves (b) for GA inversion. The group-velocity estimates for the EEP (●) are shown for reference. This set of models and curves also gives an indication of the span of the model and data space included in the GA search.

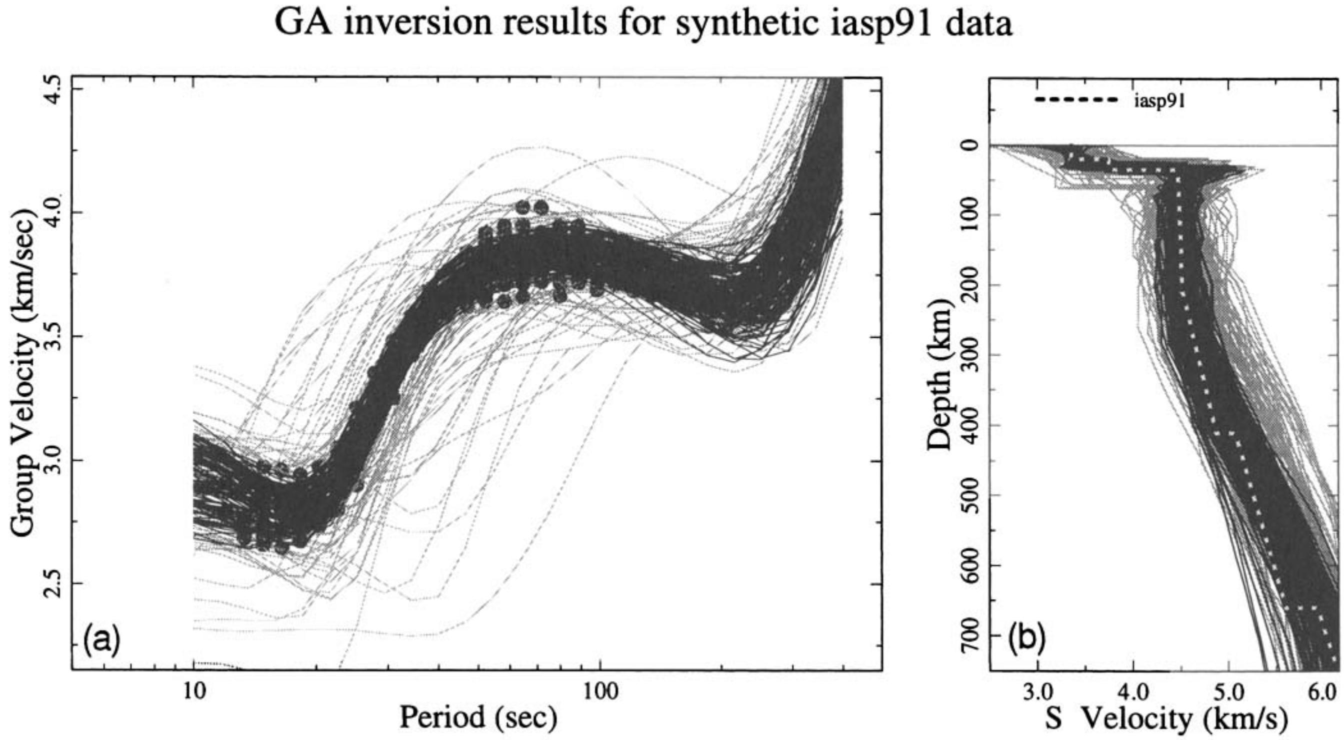

Figure 7. Results from one GA inversion for the synthetic, iasp91 data showing (a) dispersion data (●) and a representative set of synthetic dispersion curves and (b) corresponding earth models. Acceptable results are drawn with solid black lines, and a random sample of all tested results are plotted in grey. The GA tested about 4500 models from a model space with about 10^{45} members using a population size of 60 and 200 generations (because of the low crossover and mutation rates, only about one-third of the models in each generation are new).

constrained by the inversion. This lack of constraint has several causes. First, the lack of group-velocity data at periods less than about 10 s and greater than about 300 s leads to the fanning of solutions at the top and bottom of the model; below about 550 km the scatter of acceptable solutions is nearly as broad as the scatter of all models tested, indicating that the data impose almost no constraint in this region. Secondly, the physics of the forward problem smooths and obscures information about the model. This process results in the scatter in models at the top of the mantle, which reflects the physical limitations in resolving a first-order discontinuity with fundamental-mode dispersion data alone. A third cause of scatter in the models is the scatter in the data. This effect is present at all depths in the model and at all periods in the data and is difficult to distinguish from the other causes of scatter mentioned above.

In the depth range from the surface to about 350 km, the set of acceptable solutions brackets the iasp91 S-velocity model. The scatter of acceptable solutions in this depth range is typically within $\pm 0.25\,\mathrm{km\,s^{-1}}$, except for just above and just below the Moho discontinuity.

Fig. 8 shows the acceptable models and their $\pm 1\sigma$ and $\pm 2\sigma$ spread in velocity at each depth from three GA runs with the synthetic data. Allowing for differences in parametrization in the crust and at the '400' km discontinuity between the iasp91 model and the nodal models used for inversion, and the noise added to the data, the $\pm 1\sigma$ spread of acceptable models shows excellent recovery of the original iasp91 model. These results show that the processing steps and inversion method used in this work produce an unbiased estimate of the input velocity model, and they indicate the degree of scatter and uncertainty of acceptable models to be expected in the inversion of the actual data. However, the observed EEP and TE seismograms most likely do not represent wave propagation through a simple, layered earth; this synthetic test does not indicate the uncertainties or biases that may be contained in 'average' models that are produced in the inversion of real data from a laterally varying structure.

INVERSION RESULTS FOR TECTONIC EUROPE AND THE EAST EUROPEAN PLATFORM

Fig. 9 shows the results from the GA applied to the EEP data. The distribution of acceptable models (solid lines) and corresponding dispersion curves shows the mapping of uncertainty between the data space and the model space. As above, acceptable models are defined as those models giving predicted group-velocity values with an rms misfit in group velocity less than $0.85E_{\mathrm{d}}$.

The acceptable models define a Moho discontinuity at around 35–40 km depth. As with the noisy synthetic data discussed above, the scatter of acceptable models is lowest from just below the Moho to about 350 km depth. This indicates the depth range where the velocity is best constrained by the dispersion data; the scatter in the acceptable models in this depth range is about $\pm 0.25\,\mathrm{km\,s^{-1}}$. Below about 350 km the models begin to fan out and span the range of all models tested. This increase in scatter shows the loss of constraint on the solutions at depth due to the lack of dispersion data at greater than about 300 s period. The variation with depth in the scatter of these models is similar

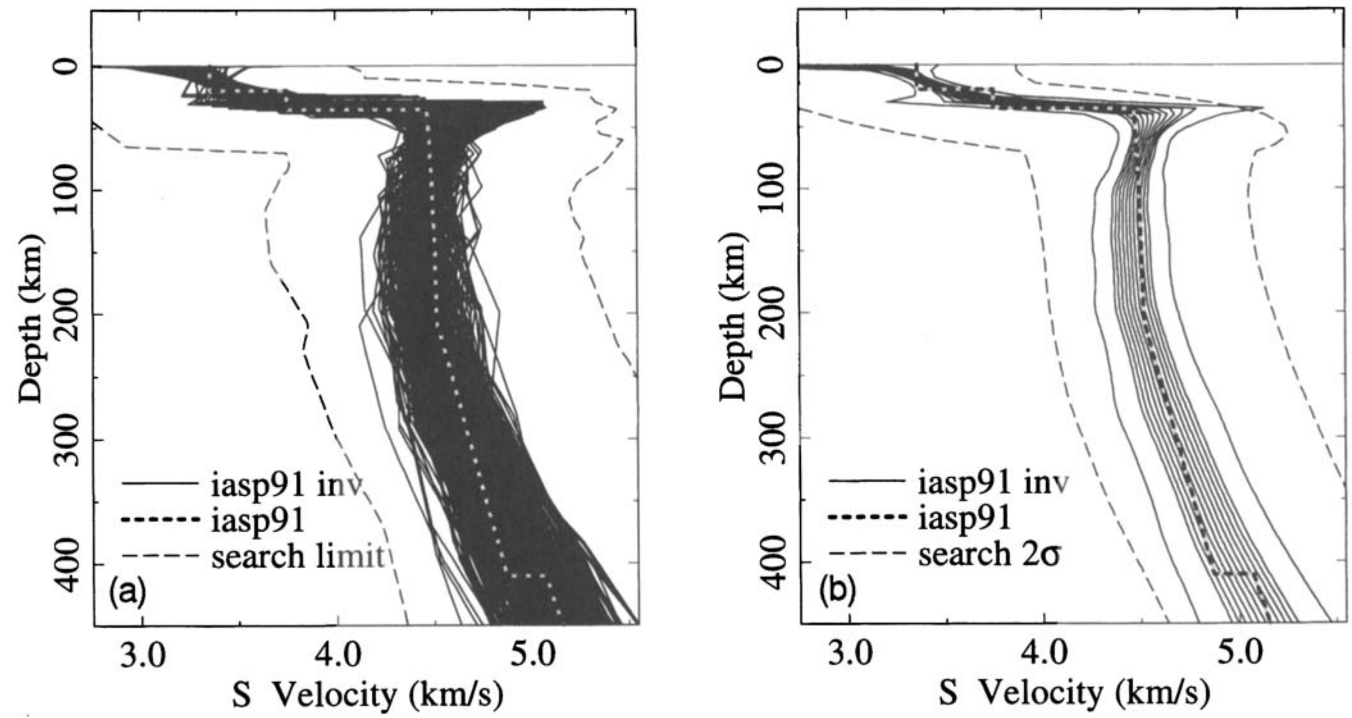

Figure 8. Upper 450 km of results from three GA runs for the synthetic iasp91 data showing (a) all acceptable models (misfit $\leq 0.85E_d$) and the approximate search limits, and (b) the $\pm 1\sigma$ spread (closely spaced solid lines) and the $\pm 2\sigma$ spread (outer solid lines) in *S* velocity at each depth for the acceptable models and the $\pm 2\sigma$ spread of the search. The search limits show the extremal velocity values at each depth of 1000 randomly generated models; the $\pm 2\sigma$ spread of the search is calculated from the same set of random models.

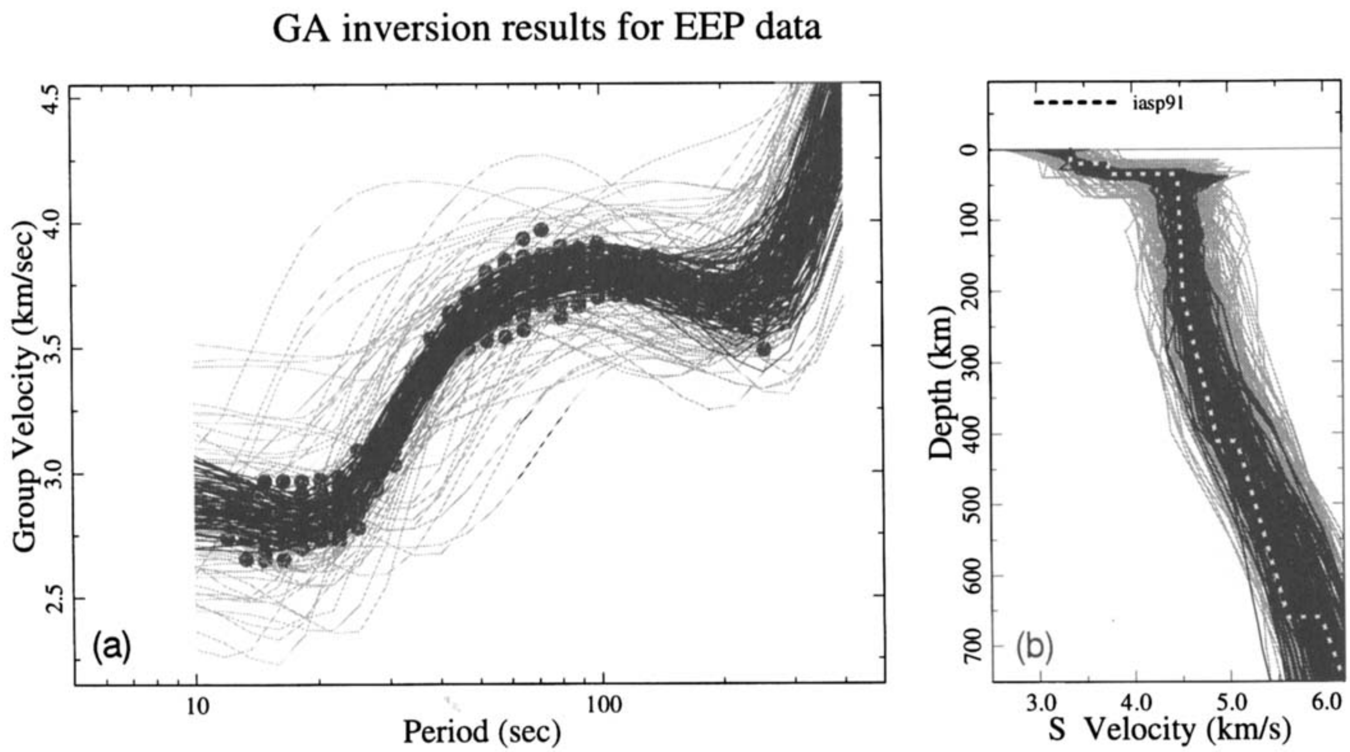

Figure 9. Results from one GA inversion for the EEP data showing (a) dispersion data (●) and a representative set of synthetic dispersion curves and (b) corresponding earth models. Acceptable results are drawn with solid black lines, and a random sample of all tested results are plotted in grey. The GA tested about 4500 models from a model space with about 10^{45} members using a population size of 60 and 200 generations (because of the low crossover and mutation rates, only about one-third of the models in each generation are new).

to that for the synthetic data because both data sets have a similar distribution of noise. The scattered EEP solutions also bracket the iasp91 model at most depths. This result indicates that the 'average' crustal and upper mantle S-velocity structure under the EEP is not distinguishable from the iasp91 model, given the data and inversion method presented here. Also, a low-velocity zone in the upper mantle is not required to fit the data.

Fig. 10 shows the results from the GA applied to the TE data. The acceptable models show a Moho discontinuity at about 25–30 km depth and a well-defined upper mantle structure to a depth of about 150 km which consists of a high-velocity 'lid' above a low-velocity zone. The scatter in the acceptable models in this depth range is about $\pm 0.35\,\mathrm{km\,s^{-1}}$. Below about 150 km the scatter in acceptable models increases; it spans the range of models tested below about 250 km depth, indicating a lack of constraint on the solutions. Because of this lack of constraint, the depth extent of the low-velocity zone under TE cannot be determined with these results. The scattered TE solutions show that, on 'average', the crust under TE is thinner and the upper mantle S velocities are lower than in the iasp91 model.

Fig. 11 shows a comparison of the acceptable models obtained with the GA for both TE and the EEP paths. This comparison indicates that a change in crustal thickness and in upper mantle S velocity across the TTZ are the main features required to explain the differences between the dispersion curves for the two regions. The spreads in crustal thickness for TE and the EEP are about 25–30 km and 35–40 km, respectively, which are in very good agreement with average Moho depths inferred previously for the two regions (Guterch *et al.* 1986; Meissner 1986). The velocity structures in the upper mantle are well constrained in both regions down to a depth of about 150 km and show about 7 per cent higher average S-wave velocities under the EEP than under TE in the upper 100 km of the mantle. The scatter in the acceptable models in this depth range gives a 2σ uncertainty in the velocity estimates of about $\pm 0.2\,\mathrm{km\,s^{-1}}$ for the EEP and about $\pm 0.25\,\mathrm{km\,s^{-1}}$ for TE. (It should be recalled that this uncertainty corresponds to an acceptance level chosen so that the scatter of the calculated dispersion curves falls within the scatter of the data values.) Because the TE results are not well constrained below about 150 km, the apparent higher velocities obtained for TE than for the EEP below about 200 km cannot be taken with confidence.

The acceptable models for the EEP have more diversity in structure near the Moho than do the TE models. Some EEP models have a strong, deeper Moho discontinuity and a distinct, thin, high-velocity lid, while other models have a weaker Moho discontinuity at shallower depth and a thicker high-velocity lid (Fig. 12). These trade-offs between Moho depth, strength of Moho contrast, lid velocity and lid thickness indicate the inability of the dispersion data to define uniquely the Moho and uppermost mantle below the EEP. The liberal parametrization and large number of solutions produced with the GA inversion give a clear illustration of possible structures near the Moho and their trade-offs; a different inversion method which required, for example, a fixed crustal structure and Moho depth would probably define only one of these structures and none of the trade-offs.

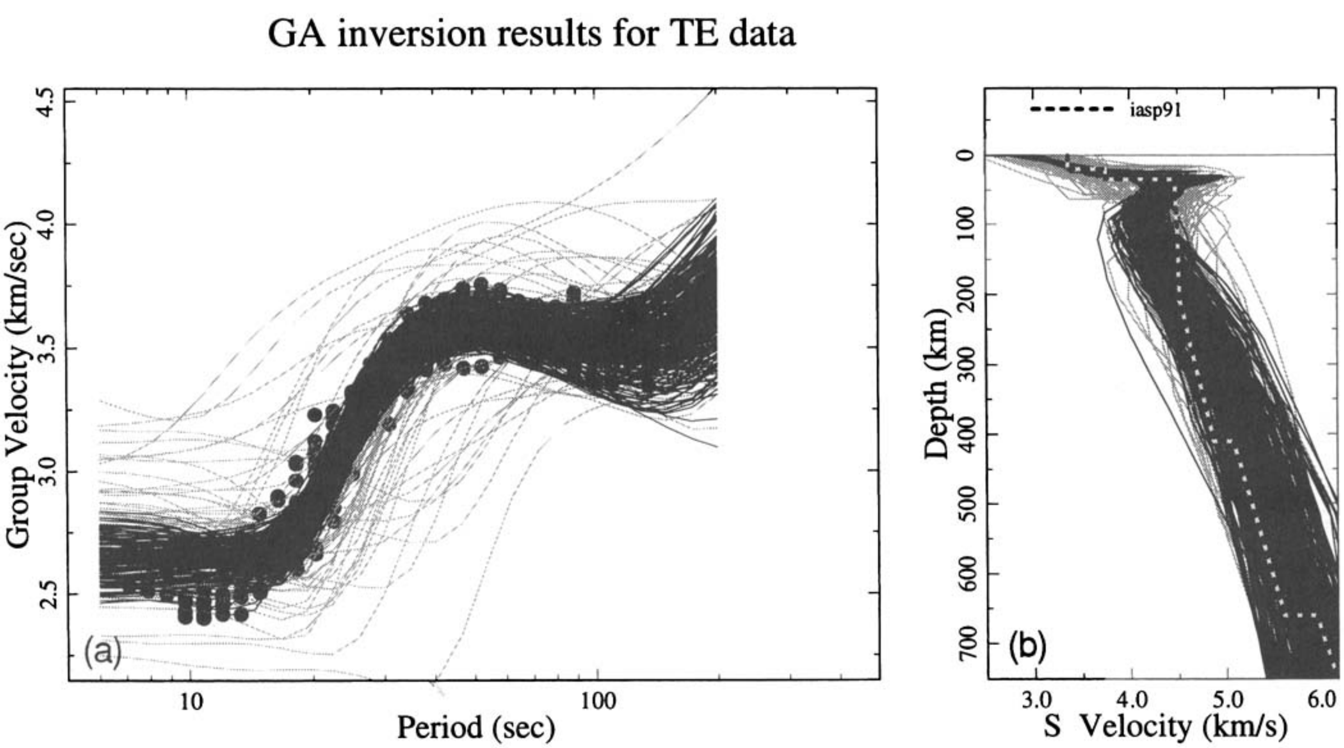

Figure 10. Results from one GA inversion for the TE data showing (a) dispersion data (●) and a representative set of synthetic dispersion curves and (b) corresponding earth models. Acceptable results are drawn with solid black lines, and a random sample of all tested results are plotted in grey. The GA tested about 4500 models from a model space with about 10^{45} members using a population size of 60 and 200 generations (because of the low crossover and mutation rates, only about one-third of the models in each generation are new).

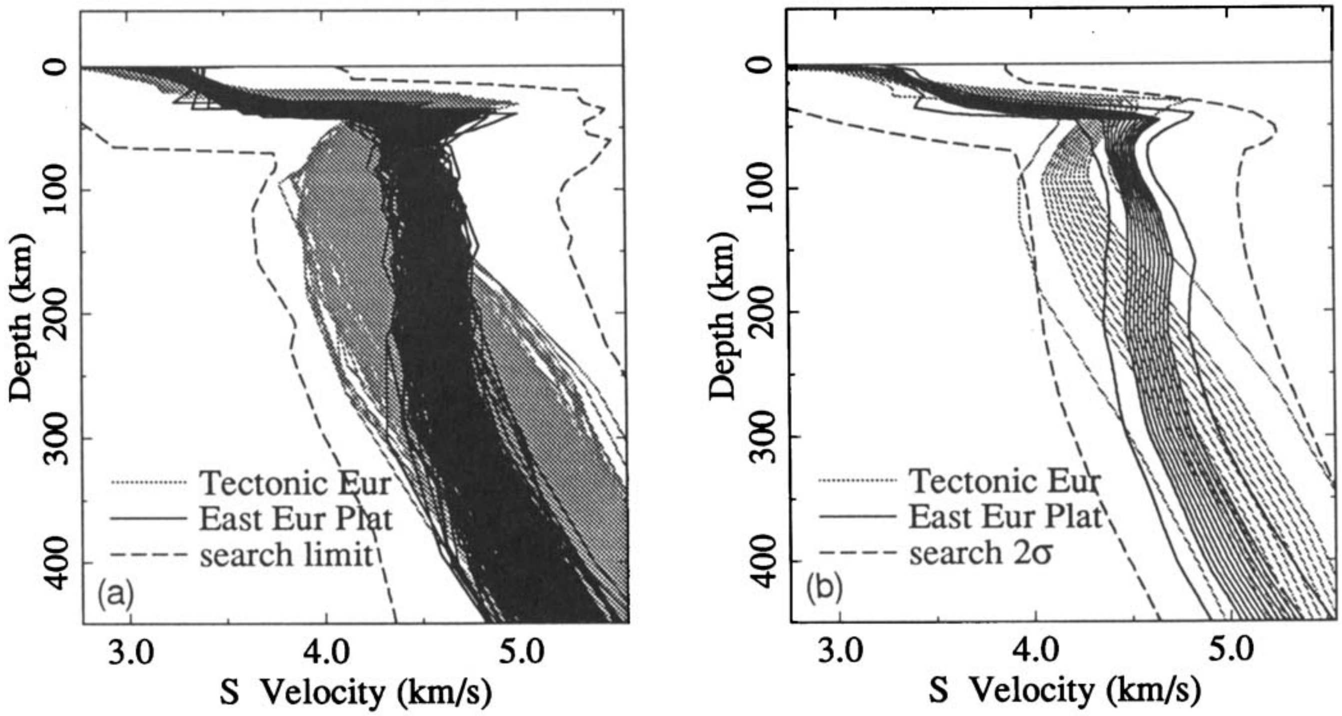

Figure 11. Comparison of the upper 450 km of results from three GA runs for the EEP and TE showing (a) all acceptable models (misfit $\leq 0.85E_d$) and the approximate search limits, and (b) the $\pm 1\sigma$ spread (closely spaced solid lines) and the $\pm 2\sigma$ spread (outer solid lines) in S velocity at each depth for the acceptable models and the $\pm 2\sigma$ spread of the search. The search limits show the extremal velocity values at each depth of 1000 randomly generated models; the $\pm 2\sigma$ spread of the search is calculated from the same set of random models. The $\pm 2\sigma$ spread of the TE results exceeds 0.5 times the $\pm 2\sigma$ spread of the search below about 150 km depth; this indicates little resolution below about 150 km for TE.

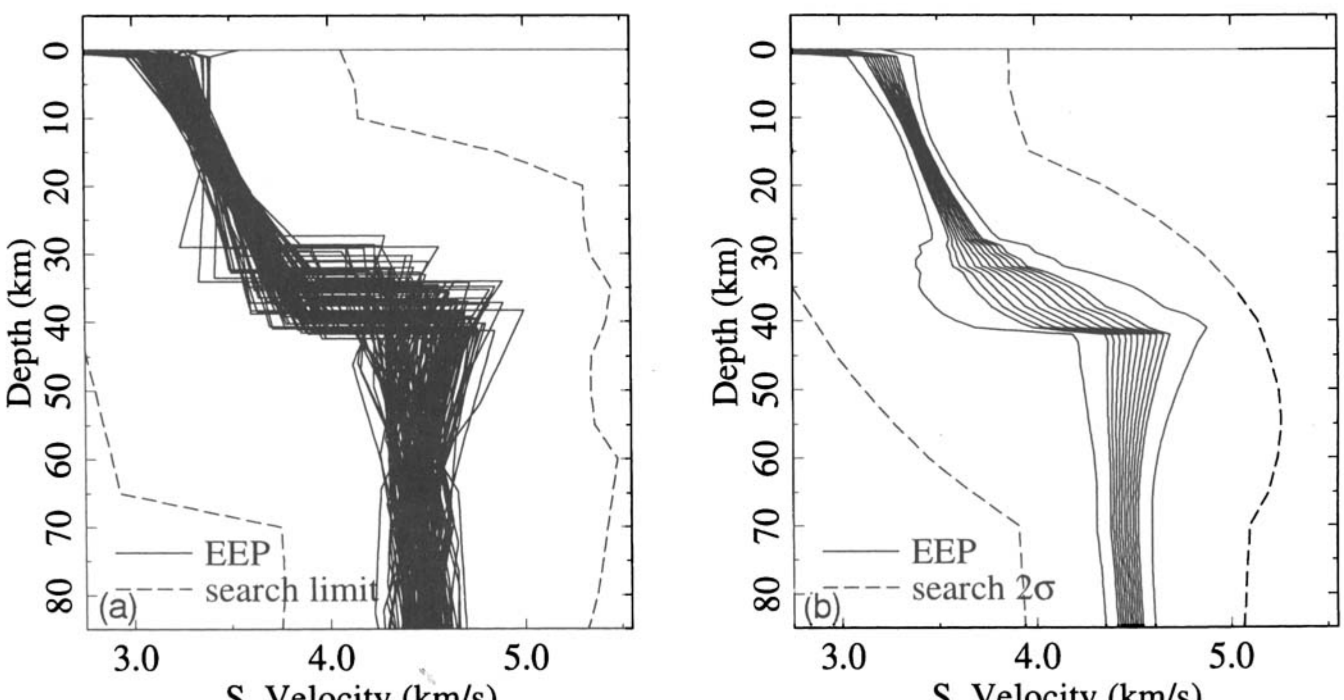

Figure 12. The upper 85 km of results from three GA runs for the EEP showing (a) all acceptable models (misfit $\leq 0.85E_d$) and the approximate search limits, and (b) the $\pm 1\sigma$ spread (closely spaced solid lines) and the $\pm 2\sigma$ spread (outer solid lines) in S velocity at each depth for the acceptable models. The search limits show the extremal velocity values at each depth of 1000 randomly generated models; the $\pm 2\sigma$ spread of the search is calculated from the same set of random models.

COMPARISON WITH CANADIAN SHIELD AND PACIFIC OCEAN STRUCTURES

To place the *S*-velocity models that we have obtained for TE and the EEP in a global context, we compare them with GA inversions of dispersion data from paths across the Canadian Shield and across the Pacific Ocean. We invert a small number of paths from each of these regions using the same techniques and nearly the same parametrization for group-velocity estimation and GA inversion as used for TE and the EEP. The only important difference is in the parametrization of the crust for the Pacific Ocean inversion, where we use a Moho depth range of 1–20 km instead of 15–70 km to allow for a thin oceanic crust, and we allow liquid layers at the top of the model. Because these additional inversions use only a small portion of the potential data set from each region, the resulting models are used here only for a general comparison with the EEP and TE. Also, in the Pacific Ocean inversion we combine paths from regions with different ages of lithosphere; in a more complete study, data from these regions should be inverted separately. The scatter of models obtained here for the Canadian Shield and for the Pacific show *S*-velocity profiles which are compatible with the results obtained in previous surface-wave studies for these regions (e.g. Brune & Dorman 1963; Cara 1979).

Fig. 13 shows the spread of acceptable models for the Canadian Shield inversion along with the results for the EEP. Within the scatter of the solutions defined at the 1σ level, the mantle velocity profiles for the two regions are indistinguishable. The only significant difference is higher velocities in the crust for the Canadian Shield than for the EEP. This difference may be caused by widespread, low-velocity sedimentary cover on the EEP that is not found on the Canadian Shield; the mid- and lower-crustal *S* velocities may be similar in the two regions. The present inversion does not test for this possibility because a discontinuity within the crust is not allowed for in the model parametrization.

Fig. 14 shows the spread of acceptable models from the Pacific Ocean paths, along with the TE results. As expected, the crustal portions of the Pacific Ocean path models are very different from the crust in the TE models. However, the mantle profile for TE is similar to that for the Pacific paths from about 50 km to 150 km depth, the greatest depth that is well constrained by the TE data.

These comparisons indicate that the upper mantle *S*-velocity structure under the EEP resembles that from a stable shield, while the adjacent TE region has upper mantle *S* velocities similar to that under young and intermediate-age oceans. These similarities are compatible with the general tectonic and geological character of the two regions: the EEP is characterized as a stable platform or shield with crystalline basement, while TE is tectonically active, with many young structural features (Meissner 1986). In a surface-wave group-velocity study of Eurasia, Feng & Teng (1983) note a similar relation between high and low upper mantle *S* velocities and stable and tectonically active regions, respectively.

DISCUSSION

Using a genetic algorithm to invert group dispersion estimates, we find a significant difference in 'average' upper mantle *S* velocity between TE and the EEP and we are able to give

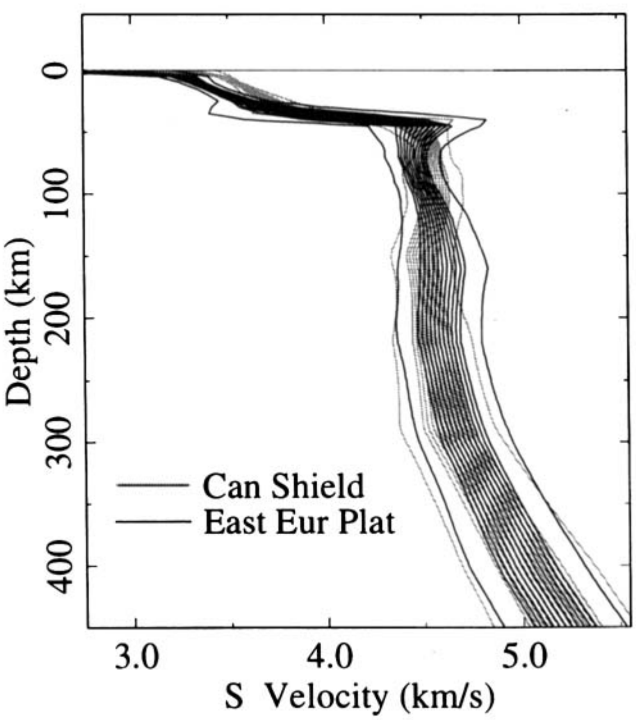

Figure 13. Comparison of the upper 450 km of results from three GA runs for the EEP and CAN showing the $\pm 1\sigma$ (closely spaced lines) and the $\pm 2\sigma$ (outer lines) spread in *S* velocity at each depth for the acceptable models.

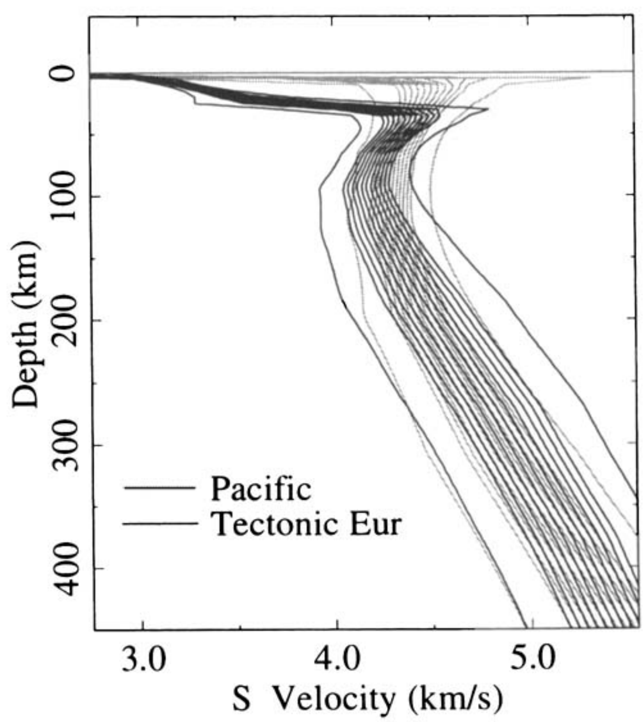

Figure 14. Comparison of the upper 450 km of results from three GA runs for the TE and PAC showing the $\pm 1\sigma$ (closely spaced lines) and the $\pm 2\sigma$ (outer lines) spread in *S* velocity at each depth for the acceptable models. The spread indicates little resolution below about 150 km for TE.

direct and useful indications of the uncertainty and trade-offs in the solutions.

We configure the GA to improve the global search characteristics of the method for application to under-determined problems with multiple and poorly defined best-fitting solutions. This configuration improves the stability of the inversion, so that similar sets of acceptable solutions are obtained when the inversion is run with different GA parameters and starting populations. This stability is obtained at the expense of slower convergence and sometimes poorer-fitting best solutions relative to a GA configured for rapid convergence to an 'optimum' solution. Also, the results still show some dependence on the GA parameters; more significant modifications to the GA, or perhaps some other search method, may be required to define adequately the acceptable misfit region of the solution space for many geophysical problems.

Two sets of dispersion curves from paths on each side of the TTZ were inverted with the GA to find layered, crust and upper mantle models. The scatter in the set of acceptable models and corresponding predicted dispersion curves shows how the physics of the problem maps scattered values between the data and solution spaces. The scatter in the models indicates the depth range where the solutions are best constrained and the uncertainty in the conclusion that the upper mantle *S* velocities vary across the TTZ. In addition, the smoothing and broad resolution in depth of surface-wave modes leads to velocity–depth trade-offs in the solutions which are well illustrated here by the scatter of solutions in the vicinity of the Moho.

The results obtained here are compatible with a contrast in upper mantle *S* velocity that occurs along or near the TTZ. However, the scatter in the group dispersion estimates and the averaging by the wavefield of material properties in some 'Fresnel volume' prevents an identification with this inversion of a sharp boundary between these two regions located at the TTZ. The greatest difference between the group-velocity estimates for the upper mantle in the two regions occurs at around 80 s period; these group velocities centre on about 3.7 km s^{-1}, and a typical path length for the observed seismograms is 2000 km. The quarter-period, first Fresnel zone for waves of 80 s period and velocity 3.7 km s^{-1} at the mid-point of a 2000 km path has a half-width of about 270 km. Consequently, the dispersion estimates are compatible with a location for an upper mantle boundary between the two regions within a few hundred kilometres of the TTZ, but it cannot be confirmed from this inversion that the resolved contrast in velocity occurs along a sharp boundary, or that this boundary is coincident with the TTZ.

The 'average' *S*-velocity estimates that we obtain for the EEP and TE around a depth of 80 km closely match the typical values obtained by Zielhuis & Nolet (1994) to the east and west of the TTZ at 80 km depth in their 'partitioned waveform' inversion for 3-D structure. However, it cannot be concluded that the two sets of results are completely in agreement, because of the differences in model parametrization in the two methods, the lack of coverage to the north-east of the TTZ in Zielhuis & Nolet (1994), and the *a priori* regionalization across the TTZ used in both works (in the Zielhuis & Nolet study different reference models are used for paths on the two sides of the TTZ; it is not clear how the resolved contrast in *S* velocity across the TTZ is dependent on this *a priori* assumption).

A generalized inversion of surface-wave phase velocities for upper mantle structure in western Europe is presented by Dost (1990). This study targets the structure under a linear network of stations to the west of our path coverage of TE, but it is interesting to note that Dost finds a high-velocity lid at 80–140 km depth, while at the same depths we find a low-velocity zone for TE; Dost finds a deeper low-velocity zone at 160–220 km depth. This difference in upper mantle models may arise because the geographic region of the study of Dost (1990) is located to the west of our TE path coverage. However, it is also possible that discrepancies in the results reflect differences in the two data sets and inversion methods. There are differences in the model sensitivities and trade-offs of the different data sets (fundamental and higher mode phase velocities versus fundamental mode group velocities); the inversion techniques differ fundamentally (a linearized inversion to find perturbations to a starting model versus the GA search technique); and other factors, such as model parametrization and regularization, undoubtedly affect the results.

By applying the same processing and GA inversion method to data from other regions, we have shown the similarity in upper mantle *S*-velocity structure between TE and the eastern Pacific Ocean region, and between the EEP and the Canadian Shield. While the similarity between continental TE and an oceanic region is difficult to interpret, the results for the EEP and the Canadian Shield indicate that these two regions may be very similar in structure and genesis below the uppermost crust.

ACKNOWLEDGMENTS

We appreciate many concise and helpful comments from an anonymous reviewer. This research was supported by the Netherlands Organization for Scientific Research (NWO) through the Pionier project PGS 76-144. This is Geodynamic Research Institute (Utrecht University) publication 95.044.

REFERENCES

Blundell, D., Freeman, R. & Mueller, S., 1992. *A Continent Revealed, The European Geotraverse*, Cambridge University Press, Cambridge.

Brune, J. & Dorman, J., 1963. Seismic waves and Earth structure in the Canadian Shield, *Bull. seism. Soc. Am.*, **53**, 167–210.

Calcagnile, G. & Panza, G.F., 1978. Crust and upper mantle structure under the Baltic Shield and Barents Sea from the dispersion of Rayleigh waves, *Tectonophysics*, **47**, 59–71.

Cara, M., 1979. Lateral variations of S velocity in the upper mantle from higher Rayleigh modes, *Geophys. J. R. astr. Soc.*, **57**, 649–670.

Dost, B., 1990. Upper mantle structure under western Europe from fundamental and higher model surface waves using the NARS array, *Geophys. J. Int.*, **100**, 131–151.

Dziewonski, A., Bloch, S. & Landisman, M., 1969. A technique for the analysis of transient seismic signals, *Bull. seism. Soc. Am.*, **59**, 427–444.

Feng, C.C. & Teng, T.L., 1983. Three-dimensional crust and upper mantle structure of the Eurasian continent, *J. geophys. Res.*, **88**, 2261–2272.

Goldberg, D.E., 1989. *Genetic Algorithms in Search, Optimization and Machine Learning*, Addison-Wesley, Reading, MA.

Goldberg, D.E. & Richardson, J., 1987. Genetic algorithms with sharing for multimodal function optimization, in *Genetic Algorithms and Their Applications, Proceedings of Second International Conference on Genetic Algorithms*, pp. 41–49, ed. Grefenstette, J.J., Erlbaum, Hillsdale, NJ.

Guterch, A., Grad, M., Materzok, R. & Perchuć, E., 1986. Deep structure of the Earth's crust in the contact zone of the Palaeozoic and Precambrian platforms in Poland (Tornquist–Teisseyre Zone), *Tectonophysics,* **128**, 251–279.

Holland, J.H., 1992. *Adaptation in Natural and Artificial Systems,* MIT Press, Cambridge, MA.

Hurtig, E., Grässl, S. & Oesburg, R.-P., 1979. Velocity variations in the upper mantle beneath TE and the EEP, *Tectonophysics,* **56**, 133–144.

Jin, S. & Madariaga, R., 1993. Background velocity inversion with a genetic algorithm, *Geophys. Res. Lett.,* **20**, 93–96.

Keilis-Borok, V.I. & Yanovskaya, T.B., 1967. Inverse problems in seismology (structural review), *Geophys. J. R. astr. Soc.,* **13**, 223–234.

Kennett, B.L.N. & Engdahl, E.R., 1991. Travel times for global earthquake location and phase identification, *Geophys. J. Int.,* **105**, 429–466.

King, S., 1993. The genetics of mantle viscosity, abstract, in Geodynamics workshop in the Czech Republic, organised by Cadek, O. & Yuen, D.A., *Terra Nova,* **5**, 581.

Lomax, A.J. & Snieder, R., 1994. Finding sets of acceptable solutions with a genetic algorithm with application to surface wave group dispersion in Europe, *Geophys. Res. Lett.,* **21**, 2617–2620.

Meissner, R., 1986. *The Continental Crust,* Academic Press, Orlando.

Nolte, B. & Frazer, L.N., 1994. Vertical seismic profile inversion with genetic algorithms, *Geophys. J. Int.,* **117**, 162–178.

Sambridge, M. & Drijkoningen, G., 1992. Genetic algorithms in seismic waveform inversion, *Geophys. J. Int.,* **109**, 323–342.

Sen, M.K. & Stoffa, P.L., 1992. Rapid sampling of model space using genetic algorithms: examples from seismic waveform inversion, *Geophys. J. Int.,* **108**, 281–292.

Snieder, R.K., 1988. Large-scale waveform inversions of surface waves for lateral heterogeneity 2. Application to surface waves in Europe and the Mediterranean, *J. geophys. Res.,* **93**, 12 067–12 080.

Spakman, W., van der Lee, S. & van der Hilst, R., 1993. Travel-time tomography of the European–Mediterranean mantle down to 1400 km, *Phys. Earth planet. Inter.,* **79**, 3–74.

Stoffa, P.L. & Sen, M.K., 1991. Nonlinear multiparameter optimization using genetic algorithms: inversion of plane-wave seismograms, *Geophysics,* **56**, 1794–1810.

Takeuchi, H. & Saito, M., 1972. Seismic surface waves, in *Surface Waves and Free Oscillations,* pp. 217–295, ed. Bolt, B.A., Methods in Computational Physics, Vol. 11, Academic Press, New York.

Zielhuis, A. & Nolet, G., 1994. Shear-wave velocity variations in the upper mantle beneath central Europe, *Geophys. J. Int.,* **117**, 695–715.

Zhang, Y. & Tanimoto, T., 1993. High resolution global upper mantle structure and plate tectonics, *J. geophys. Res.,* **98**, 9793–9823.